ADVANCED ELECTRONIC MATERIALS Open Access
www.advelectronicmat.de

A Single-Stage Differential Amplifier Using Organic Electrochemical Transistors

Farnaz Fahimi Hanzaee, Ivan B. Dimov, Luke W. Gatecliff, Richard H. Bayford, George G. Malliaras, Andreas Demosthenous,* and Nick de N. Donaldson**

Organic electrochemical transistors (OECTs) are attractive devices, particularly for biomedical applications. The inherent quality of OECTs in amplifying signals, combined with the possibility of directly interfacing with biological tissue, make them unique candidates to replace recording electrodes with the added advantage of providing on-site amplification (and thus allowing them to be counted as active electrodes). While most amplifiers using OECTs are transconductance amplifiers, having voltage-to-voltage amplification is more desirable in many applications to make the output compatible with any downstream conditioning circuit. Differential recording of physiological signals has the benefit of rejecting the common-mode noise sourcing from the environment or the body itself while amplifying the desired signal. Here the considerations for and challenges of designing an OECT-based differential amplifier are discussed and a three-transistor amplifier is proposed that can provide a common-mode rejection ratio of up to ≈20 dB. To demonstrate its advantage, a differential amplifier is used to record ECG signals from a human volunteer, and the collected data is compared with recordings from a Wheatstone bridge OECT amplifier, showing the improved signal-to-noise ratio, gain, and power consumption.

1. Introduction

Since their emergence in the mid-1980s, organic electronics have provided solutions to the fabrication of flexible and stretchable circuits that are attractive for making comfortable wearable or soft implantable bioelectronic interfaces (for a chronological review, see Ref. [1]). The organic electrochemical transistor (OECT) falls under the umbrella of three-terminal organic thin-film transistors.[2,3] Poly(3,4-ethylenedioxythiophene) doped with poly(styrene sulfonate) (PEDOT:PSS) is a commercially available p-type conducting polymer that is commonly used as the active channel due to its relatively long-term stability in ambient conditions and when in contact with water and oxygen.[3–5] PEDOT:PSS is a mixed ionic/electronic conductor with a hole conductivity that can go beyond 1000 S cm^{-1}.[6] The conductive channel is placed between the drain and source electrodes and is indirectly in contact with the gate electrode through an aqueous electrolyte. PEDOT:PSS OECTs operate in depletion mode, meaning that the transistor is ON at zero gate-source voltage. As opposed to field-effect transistors, in OECTs the gate-induced charge is not restricted to the channel-electrolyte interface, and the application of a positive voltage at the gate forces the cations within the electrolyte to move into the ion-permeable channel. These cations then interact with the sulfonate groups of PSS and replace the holes in the conducting polymer. This would modulate the number of charge carriers by causing a reversible de-doping through a reduction reaction and therefore control the current flowing between the drain and source (Equation 1, where M^+ represents a cation).[4,7]

$$PEDOT^+ : PSS^- + M^+ + e^- = PEDOT + M^+ : PSS^- \quad (1)$$

F. Fahimi Hanzaee, A. Demosthenous
Department of Electronic and Electrical Engineering
University College London
London WC1E 7JE, UK
E-mail: farnaz.fahimi.19@ucl.ac.uk; a.demosthenous@ucl.ac.uk

The ORCID identification number(s) for the author(s) of this article can be found under https://doi.org/10.1002/aelm.202400755

DOI: 10.1002/aelm.202400755

I. B. Dimov, L. W. Gatecliff, G. G. Malliaras
Electrical Engineering Division
Department of Engineering
University of Cambridge
Cambridge CB3 0FA, UK

R. H. Bayford
Department of Natural Sciences
Middlesex University
London NW4 4BT, UK

N. de N. Donaldson
Implanted Devices Group
Department of Medical Physics and Biomedical Engineering
University College
London WC1E 6BT, UK
E-mail: n.donaldson@ucl.ac.uk

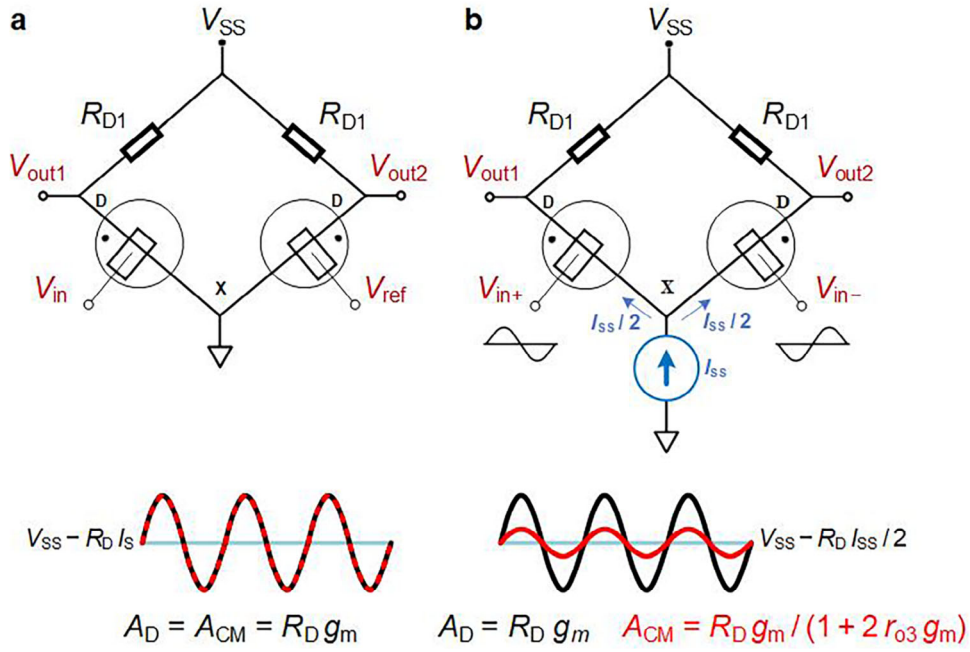

Figure 1. The architecture of differentially operated OECTs. a) An existing Wheatstone bridge configuration compared to b) this paper's proposed differential amplifier with a tail current source.

The penetration of ions into the OECT channel leads to a volumetric capacitance that makes the transconductance ($g_m = \partial I_D/\partial V_{GS}$) of this type of device much larger (≈mS) than organic field-effect transistors (≈μS), where the transconductance is limited by the interfacial charging of the channel capacitance.[8,9] This results in OECTs' small operating voltage level (<1 V) that adds to their unique properties of being biocompatible, compatible with aqueous environments, and requiring a short, low-cost, and low-temperature fabrication process.[10] As such, OECTs are suitable choices for providing local amplifications at the recording site for physiological signal measurement.

Owing to their high g_m, OECTs are mostly used as transconductance amplifiers.[11] However, in order to be compatible with the downstream processing circuitry, voltage amplifiers are more favorable in many applications. Most of the currently available OECT-based voltage amplifiers are made of a single transistor usually in a common-source (CS) configuration, and differential amplifiers are not properly explored in the field. Biomedical frontend amplifiers are typically differential since they can suppress common-mode interference while amplifying the differential information-rich signal. The requirement of an aqueous electrolyte in OECTs makes them a direct transducer between biology and electronics, giving them the combined benefit of a recording electrode and a processing amplifier. However, mismatches, performance degradation over time, and the fact that voltage drop across each pair of terminals is limited to the water electrolysis potential (i.e., 1.23 V),[12] make the design of OECT-based differential amplifiers challenging.

In this article, a single-stage three-transistor differential amplifier with OECTs is presented that can improve the amplified signal quality by providing common-mode rejection. Furthermore, the circuit and layout design considerations to improve the amplifier's common-mode rejection ratio (CMRR) and stability are discussed. Lastly, to demonstrate the benefit of the proposed amplifier in achieving higher signal-to-noise ratio (SNR), gain, and power consumption for physiological measurements, the circuit is used for ECG recording and the data is compared with signals recorded from a Wheatstone bridge OECT amplifier.

2. Experimental Section

Despite the amplification that can be offered by OECTs at the recording site, further signal processing and gain stages are necessary downstream. To address this, the output signal from an OECT-based amplifier should be compatible with the processing electronics, which typically require a voltage signal as their input. Here lies the significance of voltage-to-voltage conversion with OECTs as reported by Rivnay et al.[13] using a lithographic transistor in series with a load impedance in a CS configuration. Further studies were carried out on the same design by Braendlein and colleagues[10] when biasing the transistor in both linear and saturation regimes, demonstrating the advantage of working within saturation to achieve a higher gain. Additionally, Braendlein et al. integrated two parallel branches of OECT CS amplifiers in a Wheatstone bridge configuration (**Figure 1**a) for reference-based lactate sensing.[14] In this approach, the change of the analyte concentration in the electrolyte of the sensing OECT was compared with the fixed concentration of the reference OECT by subtracting the outputs of the two branches. This removes the common background noise that is symmetrical for both OECTs (caused by, e.g., the evaporation of the electrolytes over time or any side reactions). While this design can provide a better SNR and double the allowable output swing, the output signal swing remains dependent on the input common-mode voltage.[15] In other words, in the bridge circuit, any common-mode changes in the gate voltage alter the drain current, which in turn affects

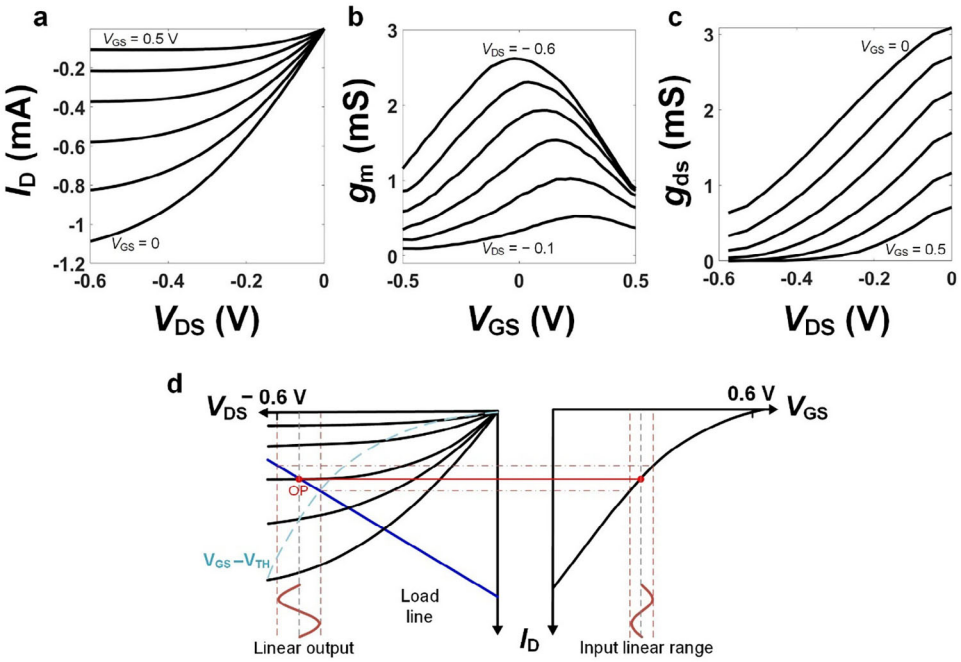

Figure 2. A depletion-mode PEDOT:PSS OECT characteristics and optimal operating point. a) An OECT's transfer curves for $0 < V_{GS} < 0.5$ V (device details discussed in Section 2.2). b) g_m versus V_{GS} for $-0.6\ V < V_{DS} < -0.1$ V, and c) g_{ds} versus V_{DS} for $0 < V_{GS} < 0.5$ V. d) Selecting the operating point within $-0.6\ V < V_{DS1,2} < V_{GS} - V_{TH}$, and the input linear range defined based on the given load line.

the output common-mode voltage level up to the point where the output either is no longer within the linear range or violates the water window.

To mitigate this dependence, a current source can be added at the source of the input transistors, fixing the current of each branch at half the total current of the source. This setup results in a single-stage differential amplifier configuration shown in Figure 1b. As described by Equations (2)–(4), in this amplifier, the paths for the differential signals (with a 180° phase difference) are the same as the ones in the Wheatstone bridge, and the gain (A_D) is similar (see Equation S1, Supporting information for further details). However, for the common-mode signals (with a 0° phase difference at the inputs), the current source output resistance (r_{o3}) should be taken into account, leading to a lower common-mode gain, A_{CM} (the gain in both cases is viewed as $V_{out1}/V_{in1} \cong V_{out2}/V_{in2}$). Consequently, A_D/A_{CM} and therefore the CMRR can be considerably improved. The role of the CMRR is particularly important in physiological measurements where the signals to both input transistors are provided from the subject's body, which could itself be a common source of interference.

Note that in the below equations, g_{m1} and g_{m2} are the transconductances of the input OECTs and should ideally be equal ($g_m = \partial I_D/\partial V_{GS}$). Also, $R_D = R_{D1} \cong R_{D2}$ is the load resistance of the amplifier, $r_o = r_{o1} \cong r_{o2} = 1/g_{ds}$ is the output impedance of the input-pair OECTs, and r_{o3} is the output impedance of the current source:

$$A_D = (R_D \| r_o)\, g_m \tag{2}$$

$$A_{CM} = \left(R_D \| r_o\right) g_m / \left(1 + 2 r_{o3} g_m\right) \tag{3}$$

$$\mathrm{CMRR} = 20\log_{10} \left|A_D/A_{CM}\right| \tag{4}$$

While g_m in OECTs is about three orders of magnitude higher than in organic field-effect transistors, the OECT's voltage gain is limited by its relatively low output impedance. The output impedance can be improved by reducing the channel width (W), length (L), and thickness, which also increases the transistor's bandwidth. However, lowering the channel thickness or W/L would in turn reduce g_m. As shown in **Figure 2**a–c, at higher $|V_{DS}|$ values, a larger g_m and a smaller transimpedance, g_{ds} ($\partial I_D/\partial V_{DS}$), can be obtained, which together result in a higher voltage gain.[10] Nonetheless, measurements show that as the voltage drop across the terminals approaches closer to the electrochemical potential of water electrolysis, the transistor's stability can be compromised and its performance can degrade faster.[12,16] This means that $\{V_{GD}, V_{DS}, V_{GS}\} < 1.23$ V should hold at all times. Therefore, in this work, $|V_{DS}|$ ($V_{DS} < 0$) was always kept below 0.6 V to stay well within the water window limit and ensure that increasing the V_{GS} up to 0.6 V would not damage the device. Also, for the transistor to remain in the saturation region, $V_{DS} < V_{GS} - V_{TH}$ should apply,[17,18] where the threshold voltage V_{TH} is typically in the range of 0.6–0.9 V (Figure S1c, Supporting information).

In the configuration of Figure 1b the dc levels of the outputs ($V_{out1,2}$) are $V_{SS} - R_D I_{SS}/2$ and a maximum gain and linear dynamic range can be achieved when the input OECTs' operation points are set within the range of $-0.6\ V < V_{DS1,2} < V_{GS} - V_{TH}$ (Figure 2d). Choosing the load impedance introduces a trade-off among the gain, input dynamic range, and power consumption. At a given operating point, increasing the resistance results in higher voltage gain but at the cost of a larger supply voltage. Also, as the load resistance is raised, the slope of the load

line decreases, restricting the allowable input range (Figure 2d). Furthermore, increasing the gain by using a higher load resistance will eventually saturate.[10] This could be due to the transistor's finite output impedance at the operating point that can reach a maximum range of tens of kΩ (Figure S1d, Supporting information).

The tail current source in Figure 1b can be replaced by an OECT biased at zero gate voltage. In this way, when $V_{G1,2} = 0$, no additional voltage other than V_{SS} is required to operate the circuit. According to Equation (3), a better CMRR can be achieved when the output impedance of the tail OECT is larger. Given the g_{ds} graph of the transistor (Figure 2c) and also that V_{GS3} is fixed at zero, the only way to increase $r_{o3} = 1/g_{ds3}$ is to operate O_3 at a higher V_{DS} value. However, the overall lower output impedance of the OECTs at zero gate voltage (< 5 kΩ; see Figure S1d, Supporting information) limits the maximum feasible CMRR. Considering $V_{G1,2} = 0$, the maximum value of $(V_{DS1,2} + V_{DS3})$ is again bound by the 1.23 V water window. Since V_{DS3} determines the V_{GS} of the input-pair OECTs, the transistors should be selected such that $I_{D1,2}(V_{GS} = V_{DS3})$ is sufficiently high to satisfy the following relationship at the set V_{DS} values:

$$I_{D3}(V_{GS} = 0) = I_{D1}(V_{GS} = -V_{DS3}) + I_{D2}(V_{GS} = -V_{DS3}) \quad (5)$$

2.1. Layout Design

As opposed to the common design approach where a global gate is used for an array of OECTs (see, e.g.,[10]), the current design requires three individually gated transistors to form a differential amplifier, ensuring that there is no crosstalk across the devices. The choice of the gate electrode can significantly influence the device's performance and therefore needs careful consideration. OECTs can be described by both an ionic-equivalent and an electronic-equivalent circuits. The latter models the electronic charge flow between the drain and source using a resistor. On the other hand, an ionic-equivalent circuit is composed of passive components in series that account for the ionic charge flow through the gate-electrolyte-channel interface via a gate-electrolyte capacitance (C_G), an electrolyte-channel capacitance (C_{ch}) and an electrolyte resistance (R_E).[4,19] It is important to ensure that C_G is considerably larger than C_{ch} so that the majority of the voltage applied to the gate is dropped across the channel and is involved in the charge modulation process for efficient gating. This can be realized by either using a non-polarizable electrode such as an Ag/AgCl pellet or by allocating a relatively large area to the gate in case it is patterned next to the channel with a polarizable metal (e.g., Au) and on the same substrate (given that $C \propto A/d$).[20] Using an external Ag/AgCl electrode immersed in the electrolyte is not always favorable, especially for wearable devices where the channels need to be gated separately.[7] As for the planar gate, coating it with a layer of PEDOT:PSS allows for a smaller footprint while having a larger C_G.[20]

To address the above considerations in this work, for each of the three transistors in an amplifier, a 5 × 5 mm^2 gate electrode coated with a ≈110 nm thick layer of PEDOT:PSS was patterned next to its channels. This resulted in an average C_G of 21 µF that is significantly larger than the C_{ch} value which is ≈8 nF (for more details regarding the ionic equivalent circuit parameter estimation please refer to Figure S2, Supporting Information, and see Ref. [8]). As shown in **Figure 3a**, four amplifiers with a similar layout were placed on a single glass slide substrate measuring 26 × 76 mm^2. The pads were connected to a set of pins to make the slide PCB-compatible and facilitate the testing process. The transistors were arranged so that the two input-pair OECTs of each amplifier were placed closer together to ensure better matching. To avoid any perturbations due to additional external wiring, the source of O_1 and O_2 were connected to the drain of O_3 at point "X" on the slide. The drain of O_1 and O_2 were connected to the pads where the two external load resistances could be attached. The point "X" was also connected to an individual pad to allow each transistor to be separately tested and characterized.

2.2. Device Fabrication

A careful fabrication procedure was followed as described in Ref. [21] To briefly review, the drains, sources, gates, and connections were patterned by first spin-coating the slide with a negative photoresist (MicroChemicals AZ nLOF 2035), exposing it to UV light using a mask aligner (SÜSS MicroTec MA/BA6), depositing 5 nm of Ti to aid with adhesion and 100 nm of Au by an e-beam evaporator (Kurt J. Lesker PVD 75), and, lastly, performing liftoff using acetone and isopropyl alcohol. After the slide was silane treated, two layers of 2 µm parylene C (PaC) were coated on the slide with an antiadhesive layer (2% Micro-90 diluted with DI water) spin-coated in between for peel-off. Subsequently, the 30 × 20 µm^2 channels, gate areas, and pads were formed by photolithography using a positive photoresist (MicroChemicals AZ 10XT), and then etching PaC with reactive-ion etching (Oxford Instruments PlasmaLab 80plus). The PEDOT:PSS dispersion was then prepared by mixing 5% (v/v) ethylene glycol and 0.25% (v/v) dodecyl benzene sulphonic acid (DBSA) with stocked PEDOT:PSS (Heraeus Epurio Clevios PH 1000) by sonication and then adding 1% (v/v) fresh (3-glycidyloxypropyl)trimethoxysilane (GOPS) as a linker. Following the treatment of the sample with oxygen plasma, the blend was filtered using a 0.45 µm polytetrafluoroethylene filter, and one layer was spin-coated on the sample at 500 rpm for 5 s and 3000 rpm for 30 s, resulting in ≈130 nm thick channels (the channels' thicknesses were estimated using electrochemical impedance spectroscopy or EIS using an Autolab PGSTAT128N potentiostat). Lastly, the top layer of the PaC was removed and the slides were hard-baked for 1 h at 130 °C and soaked in DI water overnight to remove any excessive low-molecular-weight particles. Figure 3b–d show the channel micrograph, the final sample slide, and schematics of the microfabrication layers of a transistor from the sample, respectively.

2.3. Device Characterization and Test Setup

To ensure improved stability, three considerations recommended by Bidinger et al.[22] were taken into account in preparing the devices: using fresh GOPS for fabrication, soaking the samples in DI water overnight, and preconditioning. Therefore, all transistors were preconditioned with a semiconductor parameter analyzer (Keysight B1500A) before their first use. This was performed by grounding the source and measuring the output curve (I_D vs V_{DS}) with V_{GS} changing from 0 to 0.5 V (in 7 steps) and V_{DS}

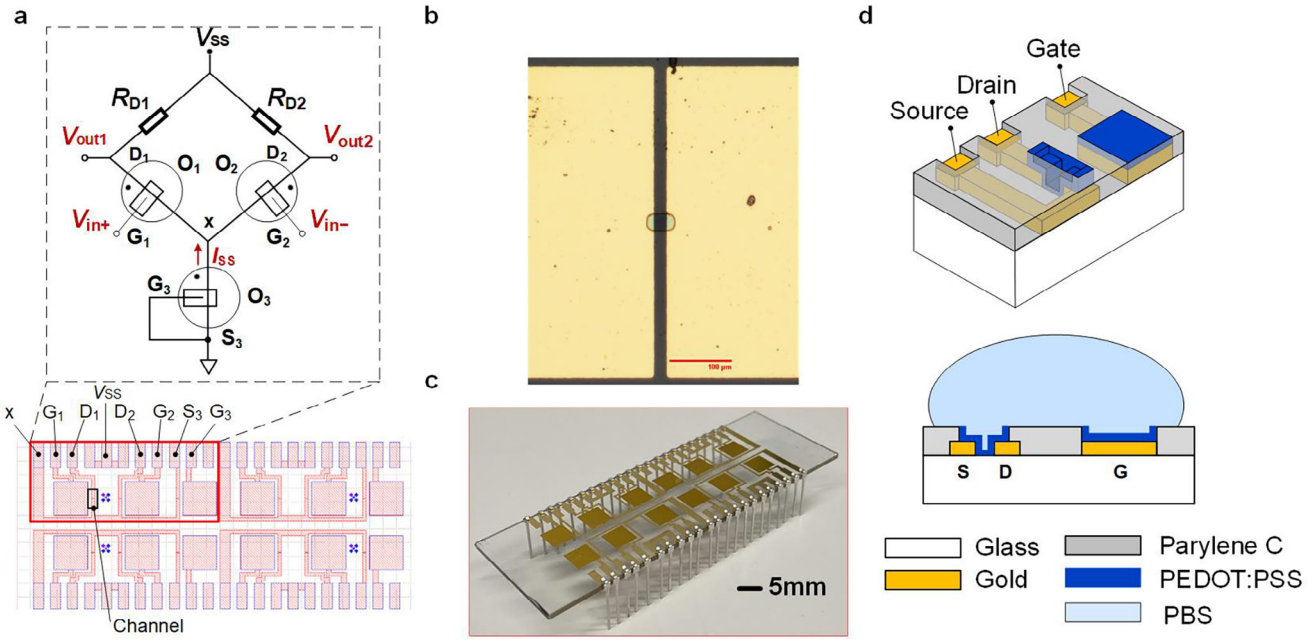

Figure 3. Schematic and fabrication of OECT amplifiers. a) The layout of four differential amplifiers (each including three OECTs) patterned on a 26 × 76 mm^2 slide. b) Optical micrograph of the channel, drain, and source of the OECT (the scale bar shows 100 µm). c) One fabricated sample with pin connectors for PCB compatibility. d) 3D and 2D cross-sectional schematics of the microfabrication layers of an OECT on the slide (not to scale).

varying between −0.6 and 0 V bidirectionally (101 steps). Preconditioning also entailed measuring the transfer curve (I_D versus V_{GS}) by bidirectionally changing V_{GS} between −0.5 and 0.5 V (51 steps) while V_{DS} ranged from −0.6 to −0.1 V (6 steps). For all the experiments, 0.01 M phosphate-buffered saline (PBS) was used as the electrolyte. PBS droplets for each transistor will remain well-separated from each other due to the hydrophobic nature of the PaC coating on the slide.

To test the OECTs in the differential amplifier configuration, a PCB was designed with two on-board potentiometers for the load resistances (Figure S3, Supporting Information). The load resistances were set to ≈5 kΩ for the amplifiers in this work to be compatible with low-power wearable biomedical systems and to ensure safety during ECG measurements. The input signals of the amplifier were applied to the gates of O_1 and O_2 using a waveform generator (RS PRO SDG1032X). The V_{SS} voltage was provided by a DC power supply and the outputs were monitored with an oscilloscope (Keysight EDUX1052A). For ECG measurements, the gates of O_1 and O_2 along with the ground (the gate of O_3) were connected to commercial electrodes (Kendall Medi-Trace) positioned on the skin through a 3-lead ECG cable with a phone jack. In addition, for safety considerations, in this case, the V_{SS} was provided by a battery-operated power supply (Figure S3, Supporting Information). The OECTs were operated with positive V_{GS} at all times to improve the stability as suggested by Keene et al.[23] All tests were performed under ambient conditions with an average temperature of 20 °C and a relative humidity of 40%.

3. Results and Discussion

Three OECTs with the output and transconductance curves shown in Figure S4 (Supporting Information) were employed in a differential amplifier configuration. The load resistances were both set at 4.9 kΩ using two potentiometers on the testing PCB, and the input transistors were initially biased at zero gate voltage. Although the input-pair OECTs had very similar characteristics, any mismatch between them could be compensated by adjusting either their gate-source voltages or the load resistances. Taking into account the limitations and considerations explained in Section 2, the goal was to set the dc levels of $V_{out1,2}$ at 1 V with 0.6 V allocated to the V_{DS} of O_1 and O_2, and a 0.4 V drop at V_{DS3}. Based on the set operating points and the given transistors' characteristics, A_D, A_{CM}, and CMRR could be calculated. The g_m values of O_1 and O_2 at the above operating points were extracted as 1.64 and 1.66 mS, respectively (Figure S4, Supporting Information). Given that the output impedances ($1/g_{ds}$) were ≈80 kΩ at this point, the differential gain could be estimated at ≈7.6 V/V using Equation (2). The output impedance of O_3 at V_{DS3} of 0.4 V was extracted to be ≈2.3 kΩ, resulting in a common-mode gain of 0.88 V/V (Equation 3), indicating a CMRR of 18.7 dB (Equation 4).

A Verilog-A model for OECTs was implemented to simulate the performance of the differential amplifier and adjust the operating points prior to measurement. The model's parameters were extracted based on the characteristics of the selected OECTs and the simulations were run in Cadence Virtuoso[18] (details of the model can be found in the supplementary document). As mentioned in Section 2.2, the transistors were fabricated with a thickness of ≈130 nm and a width and length of 30 by 20 µm. Given the process variation among the transistors, the initial resistance across the channel R_{ch} (polymer film resistance between the drain and source) of freshly fabricated OECTs, when no voltage was applied to any of the terminals, was in the range of $150\ \Omega < R_{ch} < 300\ \Omega$. Over long-term and continuous use, OECTs

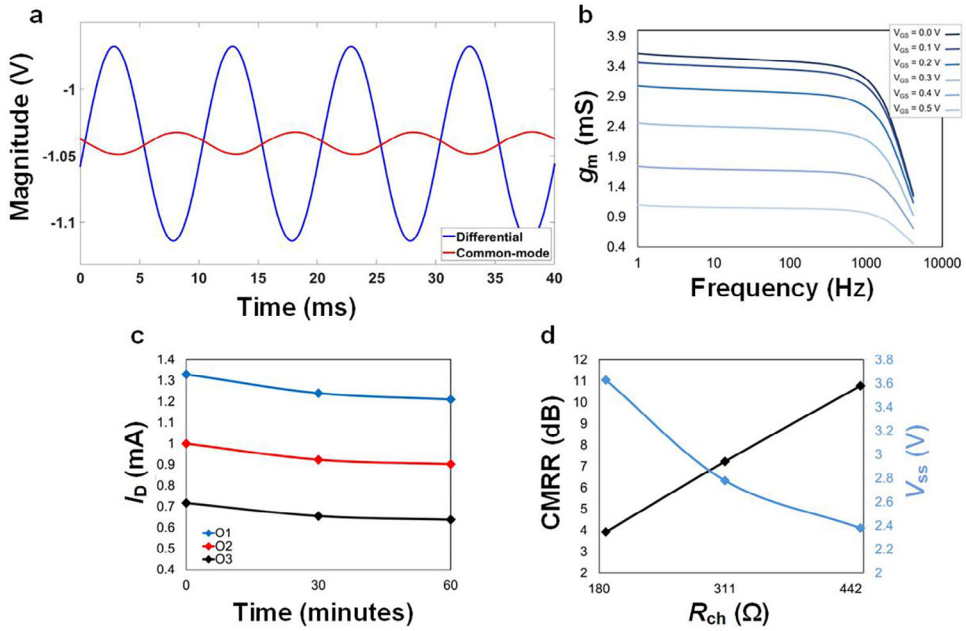

Figure 4. Measurements from OECT differential amplifiers. a) Differential-mode and common-mode outputs of the differential amplifier of Figure 1b for the input of 30 $mV_{p\text{-}p}$ at 100 Hz applied to the gates of both O_1 and O_2. b) The g_m versus frequency graphs of O_1 for $0 < V_{GS} < 0.5$ V and $V_{DS} = 0.5$ V. c) The drift of the maximum currents of three OECTs involved in a differential amplifier (O_1, O_2 and O_3 were biased at V_{GS} and V_{DS} values of 0.25 and −0.6 V, 0.33 and −0.6 V, and zero and −0.4 V, respectively), recorded after two 30-min consecutive measurements. d) The CMRR for three different OECTs (O_3) with R_{ch} values of 187, 311, and 452 Ω, with the rest of the circuit being the same. A higher CMRR was achieved for OECTs with larger R_{ch}, while a lower supply voltage was required.

gradually degrade from their initial characteristics. This could happen due to electrochemical side reactions such as oxygen reduction reactions, microstructure degradation, or small variations in the ambient conditions.[16,23–25] As a result, the channel resistance goes higher and the drain current for any corresponding gate-source and drain-source voltages decreases. As such, although the simulation could greatly help with analyzing different aspects of the amplifier, estimating the results and even improving the design, it can be expected that the measured values would be slightly different from the simulations. Using the model here, it was observed that the increase of V_{DS3}, common-mode, and differential gains upon raising the supply voltage stopped at a certain voltage level. Hence, increasing the supply voltage beyond that point would not considerably improve the amplifier's performance.

Figure 4a shows the common-mode and differential outputs (from V_{out1}) of the implemented amplifier in response to 30 $mV_{p\text{-}p}$ and 100 Hz in-phase and differential inputs applied to each $V_{in\pm}$. From the measurements, the amplifier provided a differential gain of 4.88 V/V and a common-mode gain of 0.53 V/V, leading to a CMRR of 19.2 dB. The measured voltages were $V_{DS1,2} = -0.581$ V, $V_{DS3} = -0.459$ V, $V_{G1} = 0$, $V_{G2} = 12$ mV (adjusted by the signal generator offset to ensure matching) and $V_{GS3} = 0$ when operating with a −1.8 V supply voltage. It can be observed that the drift in OECTs' characteristics from their initial values resulted in the measured gains being lower than the estimated values from both calculations and simulation, while the CMRR values remained close (simulation results are shown in Figure S5a, Supporting Information).

The output impedance of O_3 at the set operating point is ≈2.5 kΩ, and the current passing through it is 0.32 mA. Even though the tail OECT is not operating in full saturation, the fact that the I_D–V_{DS} graph's slope is reduced at the operating point makes the voltage drop at point "X" to be 0.35 V less than the case where O_3 is replaced by a resistor of the same value (i.e., −0.8 V). In addition to the lower supply voltage required when using an OECT as the tail current source rather than a single resistor, the larger voltage drop across the resistor can switch $O_{1,2}$ to the OFF state, as V_X sets the value of $V_{GS1,2}$. Also, based on the simulation, the A_D, A_{CM}, and CMRR of this circuit plateau for $V_{SS} < -1.6$ V (Figure S5b, Supporting Information). This is because, for $V_{SS} < -1.6$ V, V_{DS3} remains almost constant at 450 mV and, from the transconductance graphs of O_1 and O_2 around $V_{GS} = 450$ mV (Figure S4c,e, Supporting Information), $g_{m1,2}$ only slightly varies for -600 mV $< V_{DS1,2} < -400$ mV.

Given that any common-mode perturbation would appear as a voltage change at the gate of the input-pair OECTs, based on simulations, the performance of the above differential amplifier (with the outputs shown in Figure S5a, Supporting Information) was compared with a bridge amplifier that uses the same input transistors and load resistances. In both configurations, O_1 and O_2 were biased at the same operating points by adjusting V_{SS} (−1.35 V for the bridge amplifier and −1.8 V for the three-OECT design) and $V_{G1,2}$ to ensure similar balanced differential gains. Applying a common-mode DC voltage of 20 mV to the gate terminals of O_1 and O_2 in both amplifiers resulted in a 140 mV voltage change in the output DC level of the bridge amplifier (changing $V_{DS1,2}$ to −689 mV) thus expediting the shift of the transistors toward their safe operating limit. However, due to the CMRR

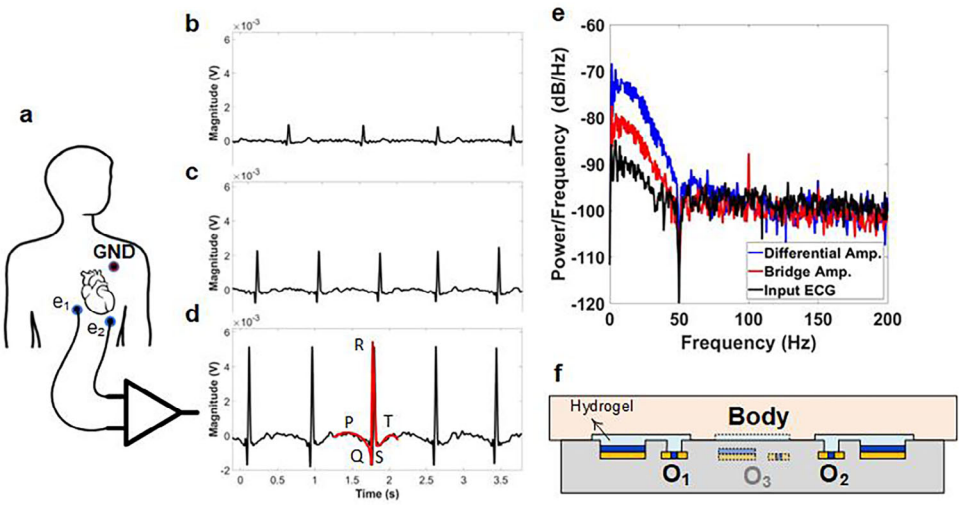

Figure 5. OECT-based ECG measurements. a) Electrode placements for ECG recording from a human heart. b) Recorded differential ECG signals with commercial electrodes (the input signal for the subsequent two amplifiers). c) Differential ECG recording from a Wheatstone bridge amplifier (gain of 3.5 V V^{-1}), and d) from the proposed differential amplifier (gain of 5.3 V V^{-1}). e) Comparison of the power spectral density of the three ECG recordings with removed dc level and the 50 Hz interference. Based on these, the SNR of the collected ECGs from commercial electrodes, the bridge amplifier, and the differential amplifier are calculated as 7, 15.8, and 21.4 dB, respectively. f) A demonstration of a possible future implementation of the three-transistor amplifier on a flexible substrate where the gates of the OECTs are placed in direct contact with the body.

offered by the proposed amplifier, in this case, the added DC voltage resulted in only a 15 mV change in the output DC level (i.e., $V_{DS1,2} + V_{DS3}$). This indicates a wider input dynamic range of the three-OECT amplifier and hence a better tolerance to any common-mode variation.

Additionally, Figure 4b illustrates the frequency response of O_1 (which is similar to O_2), suggesting that regardless of the gate-source voltage, the cutoff frequency is ≈2 kHz. This cutoff frequency is also aligned with the value estimated based on the transistor's ionic model with $R_E \approx 7.5$ kΩ and $C_G \approx 8$ nF extracted using EIS ($f_c = 1/2\pi R_E C_G$). This shows that the transistor provides a wide enough bandwidth for monitoring ECG signals that span below 150 Hz. Figure 4c depicts the degradation of three transistors that were utilized in a differential amplifier and over two 30 min of continuous measurements. In this case, the transistors O_1, O_2, and O_3 were biased at V_{GS} and V_{DS} values of 0.25 and −0.6 V, 0.33 and −0.6 V, and zero and −0.4 V, respectively. As is evident, all three transistors were subjected to a gradual irreversible degradation over time. However, the drift is sufficiently slow that the operating points would remain close to their set values during one hour of experimentation.

As pointed out earlier, the achievable CMRR can be improved when O_3 has a higher output impedance at the operating point. To demonstrate this, three transistors of different characteristics with channel resistances (R_{ch}) of 187 Ω (fresh OECT), 311 Ω, and 452 Ω (both of which were used and degraded) were incorporated as the tail transistor in an amplifier. In each case, the rest of the circuit was kept the same, and the V_{DS} values of O_1 and O_2 were set to −500 mV. Figure 4e shows that the CMRR improved from 4 to 11 dB as the R_{ch} and therefore the r_o of O_3 went up, while the required power supply (V_{SS}) decreased from 3.6 to 2.4 V. The reason for the latter was that the current level for O_3 with a higher R_{ch} is lower and thus requires a larger V_{DS3} to provide the current to O_1 and O_2. As a result, V_{GS1} and V_{GS2} go higher, which in turn can lead to smaller I_{D1} and I_{D2} values to balance the current levels that consequently lower the power consumption. Therefore, a suitable tail transistor can be chosen based on the V_{GS} and V_{DS} values set for the input-pair devices.

3.1. ECG Monitoring

To demonstrate the advantage of the proposed OECT-based differential amplifier, the circuit was used to measure ECG signals from a healthy volunteer; informed consent was obtained for the ECG recordings from the human subject (one of the authors). The results were compared with recordings from a Wheatstone bridge amplifier using the same input-pair OECTs. Note that here, as an initial proof-of-concept, the experiment was performed using OECTs fabricated on a glass substrate that was connected to the body through commercial electrodes (placed as shown in **Figure** 5a). However, the discussed differential amplifier could be implemented on a flexible and wearable substrate as well, with the gates of OECTs placed in contact with the body through a gel electrolyte. The electrodes e_1 and e_2 were connected to the gates of the input OECTs (O_1 and O_2) and e_3 was connected to the ground (GND). It is important that the skin is properly conditioned, and electrodes are placed appropriately to obtain a minimum and equal DC level at the input signals (V_{e1} and V_{e2}). This is to avoid any unexpected change in the dc levels of O_1 and O_2 and thus in the set operating points. To ensure safety during ECG measurements, a battery-operated power supply was used, and a relatively low load resistance (∼ 5 kΩ) was chosen that requires lower V_{ss} at the desired operating points. All the ECG signals in Figure 5 were conditioned in MATLAB by applying a notch filter to remove the 50 Hz powerline interference and a high-pass filter to remove the dc level. Figure 5b shows the differential input ECG signal from the electrodes ($V_{e1} - V_{e2}$), where V_{e1} and V_{e2} had dc

levels of −3 and −1.5 mV (Figure S6a, Supporting Information). Figure 5b,c demonstrate the differential ECG recordings from the outputs of the bridge amplifier and the differential amplifier ($V_{out2}-V_{out1}$), where V_{e1} and V_{e2} were applied to V_{G1} and V_{G2}, respectively (unfiltered recordings are shown in Figure S6b,c, Supporting Information). To avoid any additional biasing voltage, it is desirable to set the gate voltages of the input-pair OECTs to zero. In the case of the differential amplifier, despite the zero-gate voltage, $V_{DS3} < 0$ provides a positive V_{GS} for O_1 and O_2, and therefore they operate at a lower drain current, leading to less power consumption. As for the bridge amplifier, for the same V_{DS}, a higher current level is achieved when $V_{GS1,2} = 0$, and thus a larger power supply is required. Also, despite a larger g_m at $V_{GS} = 0$, the output impedance of the transistor is lower and could be comparable to the load resistance. Hence, the overall gain might also be lower compared to the differential amplifier.

The differential amplifier used to record the ECG signal of Figure 5d was operated by a −1.7 V supply voltage, where 460 mV was allocated to $V_{DS1,2}$ and 330 mV to V_{DS3} (here the operating points were chosen more conservatively to ensure the electrodes' dc levels would not damage the devices). The load resistances were slightly adjusted to 4.88 and 4.67 kΩ to achieve symmetrical outputs without changing $V_{G1,2}$ offsets. The differential amplifier provided an $A_D = 5.3\ V\ V^{-1}$ and an $A_{CM} = 1.1\ V\ V^{-1}$, resulting in a CMRR = 13.65 dB. On the other hand, to adjust the V_{DS} of the OECTs in the bridge amplifier at 460 mV when $V_{G1,2} = 0$, a supply voltage of 4 V was required, and the gain achieved was $A_D = 3.5\ V\ V^{-1}$ (Figure 5c).

Figure 5e shows the power spectral density of the three ECG recordings of Figure 5b–d, where the dc and the 50 Hz interference were removed. The SNR for the differential ECG from the commercial electrodes (input), the bridge amplifier, and the proposed differential amplifier were calculated as 7, 15.8, and 21.4 dB, respectively. This shows a 5.6 dB improvement over the bridge amplifier's output in the SNR for more than two times lower supply voltage when using the differential amplifier configuration. Lastly, Figure 5f provides a demonstration of a potential future direction for implementing the proposed amplifier on a flexible substrate that could be used as an ECG recording pad. As mentioned earlier, in this case, the gates of the OECTs can be placed in direct contact with the body using hydrogel as the electrolyte.

4. Conclusion

A novel OECT-based differential voltage amplifier was proposed in this paper with applications for on-site recording and amplification of physiological signals. This work is a proof of concept, discussing the potential of using OECTs in a differential amplifier configuration with common-mode rejection. The amplifier can currently offer a CMRR of ≈20 dB which helps to improve the SNR by mitigating common-mode interference. Matching between the input-pair OECTs and the stability of the transistors are important factors in this design. It was demonstrated that despite the drift of OECTs during constant measurement, given a proper fabrication methodology, the transistors could work close to their set operating points in the course of the experiment. Moreover, the matching between the input OECTs was improved by placing them in close proximity to ensure an even film thickness of the channels in both devices. The maximum achievable CMRR is dependent on the input OECTs' $g_{m1,2}$ and $r_{o1,2}$ along with r_{o3} and the load resistances. Choosing an OECT with a sufficiently large channel resistance (R_{ch}) as the tail transistor (O_3) results in a larger r_{o3} and can thus improve the CMRR. This also raises the value of $|V_{DS3}|$ and therefore increases $V_{GS1,2}$ (given that $V_{G1,2} = 0$ V). As such, a lower $I_{D1,2}$ and $g_{m1,2}$, a larger $r_{o1,2}$, and less power consumption are expected for a set V_{DS}. Grounding the gate of the tail OECT eliminates the need for any additional biasing circuitry other than the main power supply. However, the overall low r_o of the transistor at $V_{GS} = 0$ V limits the CMRR. To obtain a large voltage gain, the load resistances ($R_{D1,2}$) can be increased at the cost of a higher supply voltage and a narrower bandwidth. While it is beneficial for all three transistors involved in the amplifier to be operated at a higher $|V_{DS}|$ level (due to the increase in their r_o), the water window limits the maximum voltage drop across the terminals and should be accounted for in the design. Moreover, simulations show that for a given load resistance, the increase in the gain and CMRR, as the absolute value of V_{SS} goes higher, plateaus after a certain voltage, and increasing$|V_{SS}|$ beyond that point will not add much to the performance of the amplifier.

Lastly, a differential amplifier with a 13.65 dB CMRR was used for ECG measurements from a human volunteer. The recordings were compared with data collected using a Wheatstone bridge amplifier with the same input OECTs. The results demonstrated that the proposed differential amplifier could improve the SNR and input dynamic range while providing a higher voltage gain using less than half of the supply voltage required for the bridge amplifier. The presented amplifier has the potential to be fabricated on a flexible substrate, allowing the OECTs' channels to contact the body through a gel electrolyte and thereby eliminating the need for external recording electrodes. Whether utilized as a voltage or transconductance amplifier, the advantages offered by the proposed three-OECT configuration could also advance signal quality in a variety of other applications such as implanted or cutaneous recording and biosensing (where a single OECT is normally used). Additionally, given suitable gate-source biasing, the same configuration can be implemented using enhancement-mode OECTs. It is hoped that this work will contribute to the development of more advanced signal conditioning circuits with OECTs, enabling them to fulfil their potential in low-power biomedical applications.

Supporting Information

Supporting Information is available from the Wiley Online Library or from the author.

Acknowledgements

This work was supported by the Engineering and Physical Sciences Research Council (EPSRC) under grants EP/T001259/1 and EP/T004908/1. The authors would like to thank Sanggil Han, Stefany Kissovsky, and members of the Cambridge Bioelectronics Laboratory for their assistance with device fabrication.

Conflict of Interest

The authors declare no conflicts of interest.

Ethics Approval

All in vivo experiments were performed with the approval of the Ethics Committee of the Department of Engineering at the University of Cambridge (06/09/2018, IONBIKE) and after obtaining informed consent from volunteers.

Data Availability Statement

The data that support the findings of this study are available in the supplementary material of this article.

Keywords

common-mode rejection ratio, differential amplifier, ECG recording, OECT, organic electronics

Received: November 14, 2024
Revised: March 13, 2025
Published online:

[1] Y. Wang, S. Wustoni, J. Surgailis, Y. Zhong, A. Koklu, S. Inal, *Nat. Rev. Mater.* **2024**, *9*, 249.
[2] J. Song, H. Liu, Z. Zhao, P. Lin, F. Yan, *Adv. Mater.* **2023**, *36*, 2300034.
[3] D. A. Bernards, G. G. Malliaras, *Adv. Funct. Mater.* **2007**, *17*, 3538.
[4] J. Rivnay, S. Inal, A. Salleo, R. M. Owens, M. Berggren, G. G. Malliaras, *Nat. Rev. Mater.* **2018**, *3*, 17086.
[5] H. Sun, J. Gerasimov, M. Berggren, S. Fabiano, *J. Mater. Chem. C* **2018**, *6*, 11778.
[6] J. Rivnay, S. Inal, B. A. Collins, M. Sessolo, E. Stavrinidou, X. Strakosas, C. Tassone, D. M. Delongchamp, G. G. Malliaras, *Nat. Commun.* **2016**, *7*, 11287,.
[7] G. Tarabella, C. Santato, S. Y. Yang, S. Iannotta, G. G. Malliaras, F. Cicoira, *Appl. Phys. Lett.* **2010**, *97*, 205.
[8] D. Ohayon, V. Druet, S. Inal, *Chem. Soc. Rev.* **2023**, *52*, 1001.
[9] Y. Yao, W. Huang, J. Chen, X. Liu, L. Bai, W. Chen, Y. Cheng, J. Ping, T. J. Marks, A. Facchetti, *Adv. Mater.* **2023**, *35*, 2209906.
[10] M. Braendlein, T. Lonjaret, P. Leleux, J. M. Badier, G. G. Malliaras, *Adv. Sci.* **2017**, *4*, 1600247.
[11] J. Rivnay, P. Leleux, M. Ferro, M. Sessolo, A. Williamson, D. A. Koutsouras, D. Khodagholy, M. Ramuz, X. Strakosas, R. M. Owens, C. Benar, J.-M. Badier, C. Bernard, G. G. Malliaras, *Sci. Adv.* **2015**, *1*, 1400251.
[12] Y. Yokoyama, T. Fukutsuka, K. Miyazaki, T. Abe, *J. Electrochem. Soc.* **2018**, *165*, A3299.
[13] J. Rivnay, P. Leleux, M. Sessolo, D. Khodagholy, T. Hervé, M. Fiocchi, G. G. Malliaras, *Adv. Mater.* **2013**, *25*, 7010.
[14] M. Braendlein, A. M. Pappa, M. Ferro, A. Lopresti, C. Acquaviva, E. Mamessier, G. G. Malliaras, R. M. Ownes, *Adv. Mater.* **2017**, *29*, 1605744.
[15] B. Razavi, *Fundamentals of Microelectronics*, John Wiley & Sons, Hoboken **2021**.
[16] A. Giovannitti, R. B. Rashid, Q. Thiburce, B. D. Paulsen, C. Cendra, K. Thorley, D. Moia, J. T. Mefford, D. Hanifi, D. Weiyuan, M. Moser, A. Salleo, J. Nelson, I. McCulloch, J. Rivnay, *Adv. Mater.* **2020**, *32*, 1908047.
[17] J. T. Friedlein, R. R. McLeod, J. Rivnay, *Org. Electron.* **2018**, *63*, 398.
[18] F. F. Hanzaee, P. J. Langlois, A. Polyravas, I. B. Dimov, R. H. Bayford, G. G. Malliaras, A. Demosthenous, in 2021 IEEE Int. Midwest Symp. on Circuits and Systems (MWSCAS), IEEE, Lansing, MI **2021**, pp. 275–278.
[19] G. C. Faria, D. T. Duong, A. Salleo, *Org. Electron.* **2017**, *45*, 215.
[20] S. Han, A. G. Polyravas, S. Wustoni, S. Inal, G. G. Malliaras, *Adv. Mater. Technol.* **2021**, *6*, 2100763.
[21] A. G. Polyravas, V. F. Curto, N. Schaefer, A. B. Calia, A. Guimera-Brunet, J. A. Garrido, G. G. Malliaras, *Flex. Printed Electron.* **2019**, *4*, 044003.
[22] S. L. Bidinger, S. Han, G. G. Malliaras, T. Hasan, *Appl. Phys. Lett.* **2022**, *120*, 073302.
[23] S. T. Keene, L. W. Gatecliff, S. L. Bidinger, M. Moser, I. McCulloch, G. G. Malliaras, *MRS Commun.* **2023**, *14*, 158.
[24] G. LeCroy, C. Cendra, T. J. Quill, M. Moser, R. Hallani, J. F. Ponder, K. Stone, S. D. Kang, A. Y.-L. Liang, Q. Thiburce, I. McCulloch, F. C. Spano, A. Giovannitti, A. Salleo, *Mater. Horiz.* **2023**, *10*, 2568.
[25] A. Savva, C. Cendra, A. Giugni, B. Torre, J. Surgailis, D. Ohayon, A. Giovannitti, I. McCulloch, E. Di Fabrizio, A. Salleo, J. Rivnay, S. Inal, *Chem. Mater.* **2019**, *31*, 927.